Chemical Science

ROYAL SOCIETY OF CHEMISTRY

EDGE ARTICLE

View Article Online
View Journal | View Issue

Cite this: *Chem. Sci.*, 2024, **15**, 2197

All publication charges for this article have been paid for by the Royal Society of Chemistry

Received 27th August 2023
Accepted 23rd December 2023

DOI: 10.1039/d3sc04495e

rsc.li/chemical-science

A structure–dynamics relationship enables prediction of the water hydrogen bond exchange activation energy from experimental data†

Zeke A. Piskulich, ‡*[a] Damien Laage *[b] and Ward H. Thompson *[a]

It has long been understood that the structural features of water are determined by hydrogen bonding (H-bonding) and that the exchange of, or "jumps" between, H-bond partners underlies many of the dynamical processes in water. Despite the importance of H-bond exchanges there is, as yet, no direct method for experimentally measuring the timescale of the process or its associated activation energy. Here, we identify and exploit relationships between water's structural and dynamical properties that provide an indirect route for determining the H-bond exchange activation energy from experimental data. Specifically, we show that the enthalpy and entropy determining the radial distribution function in liquid water are linearly correlated with the activation energies for H-bond jumps, OH reorientation, and diffusion. Using temperature-dependent measurements of the radial distribution function from the literature, we demonstrate how these correlations allow us to infer the value of the jump activation energy, $E_{a,0}$, from experimental results. This analysis gives $E_{a,0}$ = 3.43 kcal mol^{-1}, which is in good agreement with that predicted by the TIP4P/2005 water model. We also illustrate other approaches for estimating this activation energy consistent with these estimates.

1 Introduction

One of the hallmarks of liquid water is its extensive hydrogen bond (H-bond) network. The ability of this network to quickly exchange these H-bonds is responsible for many of the noteworthy features of the neat liquid.[1–4] Under ambient conditions, H-bond exchanges play a critical role in most dynamical processes including diffusion,[5] reorientation,[6,7] viscosity,[8–11] dielectric relaxation,[12,13] structural rearrangements,[14,15] and chemical reactions.[16–18]

Given that these exchanges play such a ubiquitous role, it is not surprising that they have received significant attention. However, their characterization is challenging because widely used water models predict a diverse range of exchange timescales and this issue cannot be settled by experiments, which presently are unable to detect exchanges. Here we address this challenge in two ways. First, we focus on the exchange time activation energy that measures the enthalpic barrier that controls the H-bond dynamics and is a central quantity for testing and validating theories and models describing water dynamics. The activation energy naturally suffers from the same issues as the exchange time itself in that it is not directly accessible experimentally. Second, we use mechanistic insight from previous simulation studies that showed that H-bond exchanges are limited by the displacements of (the new and old) H-bond acceptors between the first and second solvation shells. The barriers for these displacements can be determined from the radial distribution function (RDF) and its temperature dependence, which *are* accessible experimentally.

Thus, in the present work we establish structure–dynamics relationships connecting the temperature dependence of the water RDF to the H-bond exchange time activation energy. These relationships are validated on other dynamical quantities, *i.e.*, reorientation and diffusion, where activation energies are experimentally accessible. Using this approach we provide the first determination of the activation energy for H-bond exchanges based on experimental structural data.

As a preliminary, it is helpful to examine some of the key developments that inform our understanding of the role of H-bond exchanges in water dynamics and their relationship to water structure. A key example of this is the development by Laage and Hynes of a theoretical treatment of these H-bond exchanges, called the extended jump model, to describe the reorientation of water molecules in terms of finite amplitude "jumps" between H-bond partners as well as a part that comes from the reorientation of the unbroken O···O "frame" vector in the unbroken H-bond.[7,19] They showed that the reorientation time τ_2, which is measured in

[a]*Department of Chemistry, University of Kansas, Lawrence, KS 66045, USA. E-mail: wthompson@ku.edu*

[b]*PASTEUR, Département de Chimie, École Normale Supérieure, PSL University, Sorbonne Université, CNRS, Paris, 75005, France. E-mail: damien.laage@ens.psl.eu*

† Electronic supplementary information (ESI) available: Activation energy data from ref. 34, linear fitting parameters, additional tests of the correlation analysis. See DOI: https://doi.org/10.1039/d3sc04495e

‡ Current address: Department of Chemistry, Boston University, Boston, MA, 02215, USA. E-mail: piskulichz@gmail.com

pump-probe infrared anisotropy experiments,[20] can be expressed in terms of these components as,

$$\frac{1}{\tau_2} = \frac{\bar{w}_2}{\tau_0} + \frac{1}{\tau_2^{\text{frame}}} \quad (1)$$

where τ_2^{frame} is the frame reorientation time, $\bar{w}_2$ is the average of a weighting function that accounts for the size of the jump angle,[21] and τ_0 is the characteristic jump time of H-bond exchanges, *i.e.*, it is the inverse of the rate constant for an OH group to switch from one H-bond acceptor to another.

More recently, Gomez *et al.* showed that the water self-diffusion coefficient can also be described in terms of a contribution associated with translational steps upon H-bond jumps and one associated with frame motion of the water and its four H-bonded partners diffusing together.[22] Analogously to the extended jump model for OH reorientation, this gives the water self-diffusion coefficient as

$$D = \frac{\bar{\rho}_{\text{O}_\text{d}} + \bar{\rho}_{\text{O}_\text{a}}}{3\tau_0} + D_{\text{frame}}, \quad (2)$$

where $\bar{\rho}_{\text{O}_\text{d}}$ and $\bar{\rho}_{\text{O}_\text{a}}$ are the average distances moved by the H-bond donor and acceptors during an H-bond exchange and D_{frame} is the frame contribution to the diffusion coefficient.

These theories indicate why, as we have shown recently, the OH reorientation time and water self-diffusion coefficient are strongly correlated with the H-bond jump time:[23] They have a common mechanistic origin. However, timescales are not easily compared (τ_0 and D do not even have the same units) and in many ways activation energies are more fundamental, adding substantially to our understanding because they represent dynamical barriers. In the same work,[23] we noted that H-bond jumps, diffusion, and reorientation all have similar, but not identical, activation energies; the differences represent the important mechanistic distinctions of each timescale. Diffusion adds the magnitude of the translation jump upon an H-bond exchange plus the "frame" diffusion of a water with its four H-bond partners intact. Reorientation of an OH group adds the magnitude of the angular jump upon an H-bond exchange plus the "frame" reorientation of the OH with its H-bond to its acceptor intact. The temperature dependences of the translation and rotational jumps are nonzero, but relatively small,[22,24] and the frame motions are themselves governed by H-bond exchanges in the surrounding waters. This gives similar (and highly correlated) activation energies for jumps, diffusion, and reorientation. The same may hold for viscosity and dielectric relaxation, but these more collective quantities do not yet have theoretical models that explicate their relation to H-bond exchanges.

A key difficulty is encountered, however, in unraveling the individual components of these jump models for water diffusion and reorientation. While the diffusion coefficient, D, and the OH reorientation time, τ_2, can be directly determined experimentally in neat water, the H-bond exchange time, τ_0, cannot. Importantly, the jump time for H-bond exchanges between two different acceptors that induced distinct, distinguishable OH stretching frequencies have been measured using two-dimensional infrared chemical exchange spectroscopy.[25,26] However, because the OH vibrational spectrum is (on average) the same before and after H-bond exchange between two equivalent water H-bond acceptors, this approach cannot be applied to neat water. For some time, it was thought that τ_0 was equal to the spectral diffusion time extracted from the frequency–frequency time correlation function accessible from two-dimensional infrared spectroscopy experiments. However, we have recently shown[27] that, in simulations, the H-bond exchange time is not currently accessible from such measurements, rather the spectral diffusion time is almost fully determined by rearrangements within intact H-bonds and transient H-bond breakages.[27] Thus, additional progress on the connection of experimental measurements to τ_0 is needed.

This motivates other approaches to using experimental data to characterize the H-bond exchange process. One approach is to use the variability in water models for molecular dynamics simulations. While any given water model obeys the relations in eqn (1) and (2), the differences in the models yields a range of timescales. We have recently shown that this leads to strong linear correlations between the (inverse) jump time and both the diffusion coefficient and the (inverse) reorientation time for nine commonly used water models.[23] These correlations are empirical in that they represent an average behavior over the different models, which, *e.g.*, each have different values of $\bar{w}_2$ and $\tau_{2,\text{frame}}$ in eqn (1). Nevertheless, one can use them to infer the jump time based on experimental data. The measured OH reorientation time is 2.6 ps,[28,29] which yields a jump time of 3.2 ps from the correlation between $1/\tau_2$ and $1/\tau_0$ shown in Fig. 1b of ref. 23. Similarly, the measured water self-diffusion coefficient is 2.30×10^{-5} cm^2 s^{-1},[30] giving a jump time of 3.8 ps from the correlation of D and $1/\tau_0$ shown in Fig. 1a of the same work. These estimates are important guide posts, but not fully satisfactory given the significant difference between the estimates based on the diffusion coefficient and reorientation time.

The considerations discussed above motivate our focus in this work on the jump time activation energy,

$$E_{\text{a},0} = -\frac{\partial \ln(1/\tau_0)}{\partial \beta}, \quad (3)$$

where $\beta = 1/(k_\text{b}T)$, k_b is Boltzmann's constant, and T is the temperature. Like the jump time itself, determining this activation energy from experimental measurements is a critical challenge to be overcome in the long-standing goal of understanding liquid water. In the following, we show how this can be accomplished by identifying the key elements of water structure that determine the enthalpic barrier to H-bond exchange.

2 Theory

The jump timescale, τ_0, measures the inverse rate constant for an OH moiety to exchange H-bond acceptors and, as is clear from the above discussion, is one of the fundamental timescales of liquid water. From a molecular simulation τ_0 can be calculated within the stable states picture[31] from the time correlation function

$$C_{ab}(t) = \langle n_a(0) n_b(t) \rangle, \quad (4)$$

where $\langle\cdots\rangle$ indicates a thermal average and n_a (n_b) is equal to 1 if the chosen OH is H-bonded to molecule a (b), and is otherwise zero. Absorbing boundary conditions are used so that after an exchange occurs, that molecule's contribution remains one regardless of whether it switches back to its original H-bond partner due to a further exchange. At longer times, $1 - C_{ab}(t) = e^{-t/\tau_0}$, enabling determination of the jump time.

We have recently developed a fluctuation theory for dynamics approach that enables the direct determination of an activation energy from simulations at a single temperature,[23,32–34] by computing the analytical derivative of a timescale or rate constant with respect to temperature, in contrast to the numerical derivative obtained in an Arrhenius analysis. Briefly, this approach uses the fact that the temperature, or more precisely the β derivative of, for example, $C_{ab}(t)$ is given by

$$\frac{\partial C_{ab}(t)}{\partial \beta} = -\langle \delta H(0) n_a(0) n_b(t)\rangle \equiv - C_{H,ab}(t), \quad (5)$$

where $\delta H(0) = H(0) - \langle H\rangle$ with H the total system Hamiltonian. In other words, the temperature derivative is related to the correlation of energy fluctuations with the dynamics; the activation energy is straightforwardly obtained by fitting $C_{H,ab}(t)$.[24] We have used this method in a recent study in which we have directly calculated the activation energies for water diffusion, OH reorientation, and H-bond exchanges for a wide range of water models.[34] Those data are used here and related to properties of the water structure.

Namely, the same approach can be used to calculate the temperature dependence of static equilibrium properties.[35–37] In liquids the RDF, for example,

$$g(r) = \frac{V}{N^2}\left\langle \sum_i \sum_{j\neq i} \delta\left(r - \left|\vec{r}_{ij}\right|\right)\right\rangle, \quad (6)$$

is frequently used to characterize liquid structure.[38] Here, $\vec{r}_{ij} = \vec{r}_j - \vec{r}_i$ is the distance between sites i and j, N is the number of molecules, r is the distance between two atoms – in this work we focus on the intermolecular O$\cdots$O coordinate to obtain $g_{OO}(r)$ – and V is the volume. Experimentally, RDFs are obtained as the Fourier transform of the structure factor measured by either neutron[39–41] or X-ray scattering.[42,43]

Using fluctuation theory, we have previously demonstrated that the derivative of the RDF with respect to temperature, or more precisely, β, can be expressed as,

$$\frac{\partial g(r)}{\partial \beta} = -\frac{V}{N^2}\left\langle \delta H \sum_i \sum_{j\neq i} \delta\left(r - \left|\vec{r}_{ij}\right|\right)\right\rangle = -g_H(r). \quad (7)$$

Here we have neglected the $p\delta V$ contribution to the derivative present in the isothermal-isobaric ensemble, which is negligible at 1 bar. This derivative is evaluated directly from simulations at a single T and p.

3 Computational methods

We have carried out simulations of the oxygen–oxygen RDF and its β derivative for nine different water models. For each model, we generated initial configurations and the necessary data files for molecular dynamics simulations using PACKMOL.[44] Initial velocities were generated from the room temperature Maxwell–Boltzmann distribution. Molecular dynamics simulations were run using the Large-Scale Atomic/Molecular Massively Parallel Simulator (LAMMPS).[45] Liquid structures were calculated from separate long trajectories, propagated for 50 ns in the NpT ensemble at 1 bar and 298.15 K after a 1 ns equilibration. For these trajectories, configurations were output every 100 fs (in total 500 000 configurations) from which the radial distribution function and its derivative were calculated.

A Nosé–Hoover thermostat and barostat were used, both of chain length 3, with damping parameters of 100 fs and 1000 fs, respectively.[46,47] For all simulations, the Particle-Particle-Particle Mesh (PPPM) Ewald summation method was used for the calculation of electrostatic interactions, with a tolerance parameter of 1×10^{-4}.[48,49] For simulations involving rigid water molecules, the SHAKE algorithm was used to hold bonds and angles constant, also with a tolerance of 1×10^{-4}.[50]

Note that the activation energies presented in this work are taken from ref. 34 and a different approach was used there. In particular, to remove the effect of the barostat and thermostat on the calculated dynamical timescales and their activation energies, they are computed from constant volume and energy (NVE) trajectories that are initiated from configurations sampled from an NpT trajectory.

Uncertainties in the structural parameters were calculated using block averages over five blocks, and represent 95% confidence intervals according to the Student's t-distribution.[51] Uncertainties for the activation energies are reproduced from ref. 34 and also represent 95% confidence interval obtained from ten blocks.

4 Results

We have calculated the oxygen–oxygen RDF for each water model listed in Table 1 and plotted the results in Fig. 1. The studied models represent a wide range of parametrizations that spans 3-site and 4-site descriptions and includes both flexible and 3-body models. In this figure, we have also included the

Table 1 $E_{a,0}$, $\Delta\Delta H^{\ddagger}_{0}$, $\Delta\Delta H^{\theta}$, and $-T\Delta\Delta S^{\ddagger}$ for each water model and experiment[43]

Model	$E_{a,0}$[a]	$\Delta\Delta H^{\ddagger}$	$\Delta\Delta H^{\ddagger}_{\theta}$	$-T\Delta\Delta S^{\ddagger}$
SPC/E[52]	3.09_4	2.58_5	0.51_7	-1.50_{10}
SPC/Fw[53]	3.27_6	2.72_9	0.55_{11}	-1.57_{14}
TIP3P[54,55]	2.71_5	2.28_3	0.43_6	-1.39_4
TIP3P/Fw[54,55]	3.38_6	2.82_7	0.56_{10}	-1.63_9
OPC3 [56]	3.26_6	2.58_8	0.68_{10}	-1.45_{11}
E3B2 [57]	4.11_6	3.71_8	0.40_{10}	-2.54_8
E3B3 [58]	4.03_2	3.58_{13}	0.45_{15}	-2.40_{16}
TIP4P/2005 [59]	3.63_5	3.25_5	0.38_8	-2.10_5
TIP4P/Ew[60]	3.52_6	3.18_8	0.34_9	-2.03_{13}
Expt[43]	3.43	2.97	0.46	−2.16

[a] Model values are reproduced from ref. 34; experimental value predicted as described in the text.

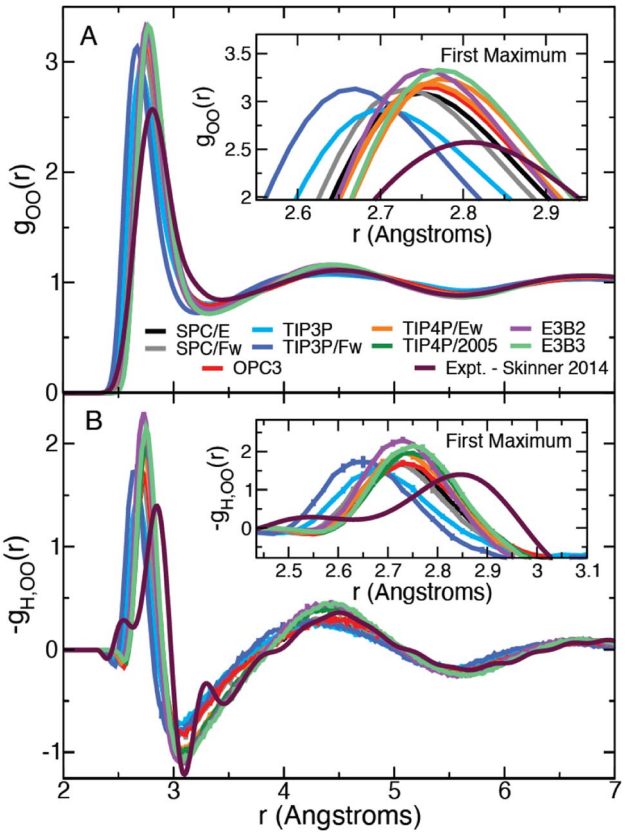

Fig. 1 Plots of the liquid water oxygen–oxygen (A) radial distribution function and (B) the β derivative of the RDF, $-g_{H,OO}(r)$, for each water model. Insets show a closer view of the first maximum.

experimental radial distribution function at 295.1 K as measured by Skinner *et al.* using X-ray diffraction.[43] In this way, the results in Fig. 1 represent a diverse array of descriptions of water. Each simulation model exhibits moderate agreement with the experimental RDF, but all overestimate the height of the first peak. The models generally agree on the peak's location along r, with the exception of the TIP3P and TIP3P/Fw models which predict a more contracted liquid structure.

We have also directly calculated the β derivative of the RDF at 298.15 K for each water model using eqn (7) and have used the experimentally measured RDFs at 307 and 284.5 K to evaluate this derivative numerically.[43] The results are plotted in Fig. 1. The model and the experimental derivatives are in general qualitative agreement though the models exhibit slightly less structure than the experimental result. Interestingly the 4-site models are in good agreement with experiment after the first minimum (located at about 3.1 Å); however, only TIP3P reproduces the height of the first maximum with the other models slightly overestimating the T-dependence of the peak.

5 Discussion

In the remainder of this Paper, we examine how these structural properties of water and their temperature dependence can provide information about the *dynamics* of water. In particular, we focus on the former, which can be used to determine the thermodynamic barriers – both enthalpic and entropic – for water rearrangements and investigate their relationships to dynamical activation energies. It is found that these provide a route to estimations of the activation energy for the H-bond exchange time.

The Gibbs free energy can be calculated from the RDF as,

$$\Delta G_{OO}(r) = -k_b T \ln g_{OO}(r) - 2k_b T \ln r, \quad (8)$$

where the first term is the potential of mean force and the second term is the entropy associated with the increasing volume with r. The calculated $\Delta G_{OO}(r)$ for each model and the experimental results of ref. 43 are shown in Fig. 2. We find that the free energy barrier to move from the first to the second solvation shell is overestimated by each model compared with experiment. Generally, we observe that a higher barrier between the first and second solvation shell corresponds with an overall shallower minimum in the second solvation shell, though the two flexible models do not follow this pattern.

It is straightforward to show[35] that the derivative given by eqn (7) applied to the OO RDF, $g_{H,OO}(r)$, can be used to determine the corresponding enthalpy,

$$\Delta H_{OO}(r) = \frac{g_{H,OO}(r)}{g_{OO}(r)}, \quad (9)$$

and the entropic contribution to the Gibbs free energy as,

$$-T\Delta S_{OO}(r) = \Delta G_{OO}(r) - \Delta H_{OO}(r), \quad (10)$$

using $\Delta G_{OO}(r) = \Delta H_{OO}(r) - T\Delta S_{OO}(r)$; the ΔH and ΔS obtained are those for 298 K and may vary with temperature though, at constant volume, we have found they are effectively independent of temperature.[35] The enthalpy and entropy contributions to the free energy calculated in this way are shown in Fig. 2. Both quantities exhibit more structuring in the experimental results than in the simulations. The experimental enthalpic barrier for moving from the first to second solvation shell is in best agreement with the E3B models, though the measured second solvation shell minimum is shallower than predicted by any of the models. The experimental entropy profile is similar to that predicted by all of the water models and agrees best with the 4-site models studied. However, at short distances the measured $-T\Delta S_{OO}(r)$ increases more steeply than in any of the models.

We have previously reported calculations of the diffusion, reorientation, and the jump activation energies for the models considered here;[34] the results are given in Table S1 in the ESI.† We now examine the relationship between the enthalpic (and entropic) change associated with exchanging an H-bond and the observed activation energy for each of these three timescales.

It should be noted that the H-bond jump involves the movement of the original acceptor out of the first solvation shell of the H-bond donor, while the new acceptor must enter the first solvation shell. Thus, it is useful to consider the quantity $\Delta\Delta H^{\ddagger} = \Delta H_f^{\ddagger} + \Delta H_b^{\ddagger}$, which corresponds to the sum of the enthalpy

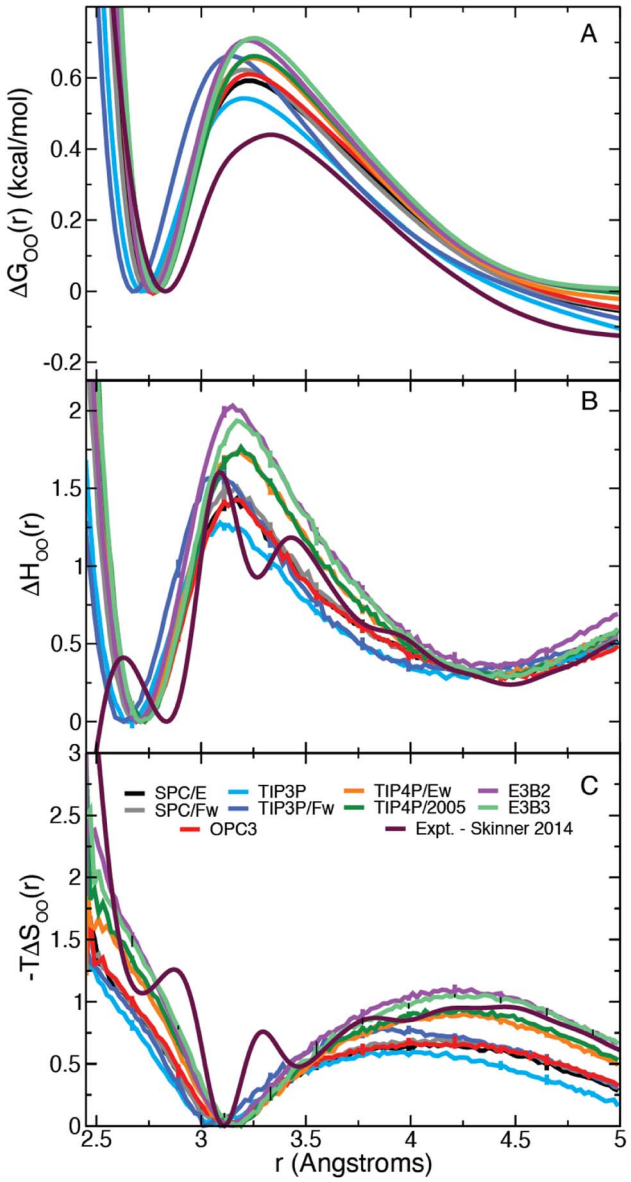

Fig. 2 (A) Gibbs free energy, (B) enthalpy, and (C) entropy as a function of the intermolecular water oxygen–oxygen (OO) distance. (The first minimum is set to zero in each case.)

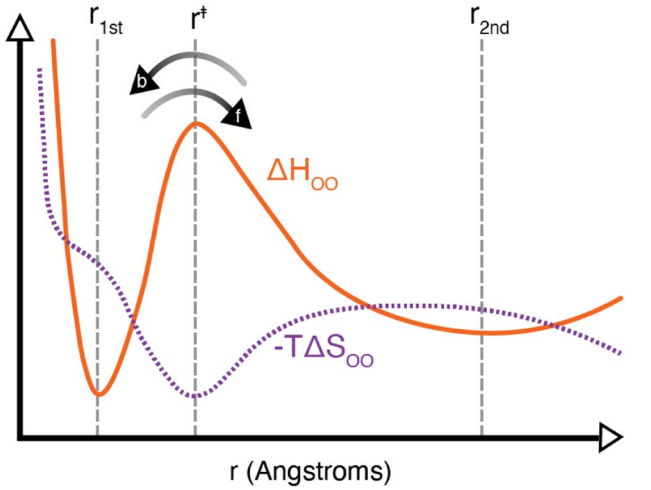

Fig. 3 Schematic of the liquid water oxygen–oxygen enthalpic (solid orange line) and entropic (dashed purple line) contributions to the free energy. Indicated on the plot are the positions r_{1st}, $r^{\ddagger}$, and r_{2nd} as well as the forward and backward directions over the enthalpic barrier. As noted in the text, an H-bond exchange must involve one water molecule leaving the first solvation shell, with an enthalpic barrier of $\Delta H_f^{\ddagger}$, and another molecule entering the first solvation shell, with an enthalpic barrier of $\Delta H_b^{\ddagger}$.

barrier in both directions, as illustrated schematically in Fig. 3. Here we define $\Delta H_f^{\ddagger}$ and $\Delta H_b^{\ddagger}$ as the enthalpy required to cross the barrier in the forward and backward directions, respectively. These are calculated as

$$\begin{aligned}\Delta H_f^{\ddagger} &= \Delta H_{OO}(r^{\ddagger}) - \Delta H_{OO}(r_{1st}) \\ \Delta H_b^{\ddagger} &= \Delta H_{OO}(r^{\ddagger}) - \Delta H_{OO}(r_{2nd}),\end{aligned} \tag{11}$$

where $r^{\ddagger}$, r_{1st}, and r_{2nd} are the positions of the transition state, the first solvation shell, and second solvation shell, respectively; see Fig. 3. A similar approach has previously been successfully used with the RDF to estimate the jump time, though it relies on information only available from simulations.[61]

Laage and Hynes have suggested previously that the jump activation energy can be expressed as $E_{a,0} = \Delta\Delta H^{\ddagger} + \Delta\Delta H_{\theta}^{\ddagger}$ where the second term corresponds to a separate barrier along an angular coordinate.[7] From our present calculations, we find that the SPC/E model $\Delta\Delta H^{\ddagger}$ is 2.58 ± 0.06 kcal mol^{-1}, and its $E_{a,0}$ is 3.09 ± 0.04 kcal mol^{-1}. Using these values, we then find $\Delta\Delta H_{\theta}^{\ddagger} = 0.51 \pm 0.07$ kcal mol^{-1} in close agreement with the result of $\sim$0.5 kcal mol^{-1} in Fig. 17 of ref. 7. In Table 1 we have included our calculated values of $\Delta\Delta H_{\theta}^{\ddagger} = E_{a,0} - \Delta\Delta H^{\ddagger}$ for each water model. Interestingly, 4-site models have generally larger values of $\Delta\Delta H^{\ddagger}$ and smaller values of $\Delta\Delta H_{\theta}^{\ddagger}$ than their 3-site brethren, leading to higher values of $E_{a,0}$.

It is useful to consider instead the dependence of a given activation energy on the enthalpic barrier $\Delta\Delta H^{\ddagger}$. We have plotted the jump, reorientation, and diffusion activation energies of each water model as a function of their corresponding values of $\Delta\Delta H^{\ddagger}$ in Fig. 4A–C. The data show a clear linear dependence between each activation energy and the structural enthalpic barrier, such that a linear function of the form

$$E_{a,X} = m_{H,X}(\Delta\Delta H^{\ddagger}) + b_{H,X}, \tag{12}$$

provides an excellent fit of the data, as also shown in Fig. 4A–C. Here, $b_{H,X}$ is the y-intercept, the value $m_{H,X}$ is the slope, and X represents the timescale, with $X = 0$ for the jump time, $X = 2$ for the reorientation time, or $X = D$ for the diffusion coefficient. The values of $m_{H,X}$ and $b_{H,X}$ are given in Table S2 in the ESI.†

These results demonstrate the clear structure–dynamics relationships for water, not only for the jump time but also for the OH reorientation time and the self-diffusion coefficient. For all three timescales $E_{a,X}$ and $\Delta\Delta H^{\ddagger}$ have a strong linear correlation (R^2 between 0.916 and 0.957). We have tabulated the fitting parameters and R^2 values for each fit in Table S2.† It is interesting to note that the slope for the jump time activation

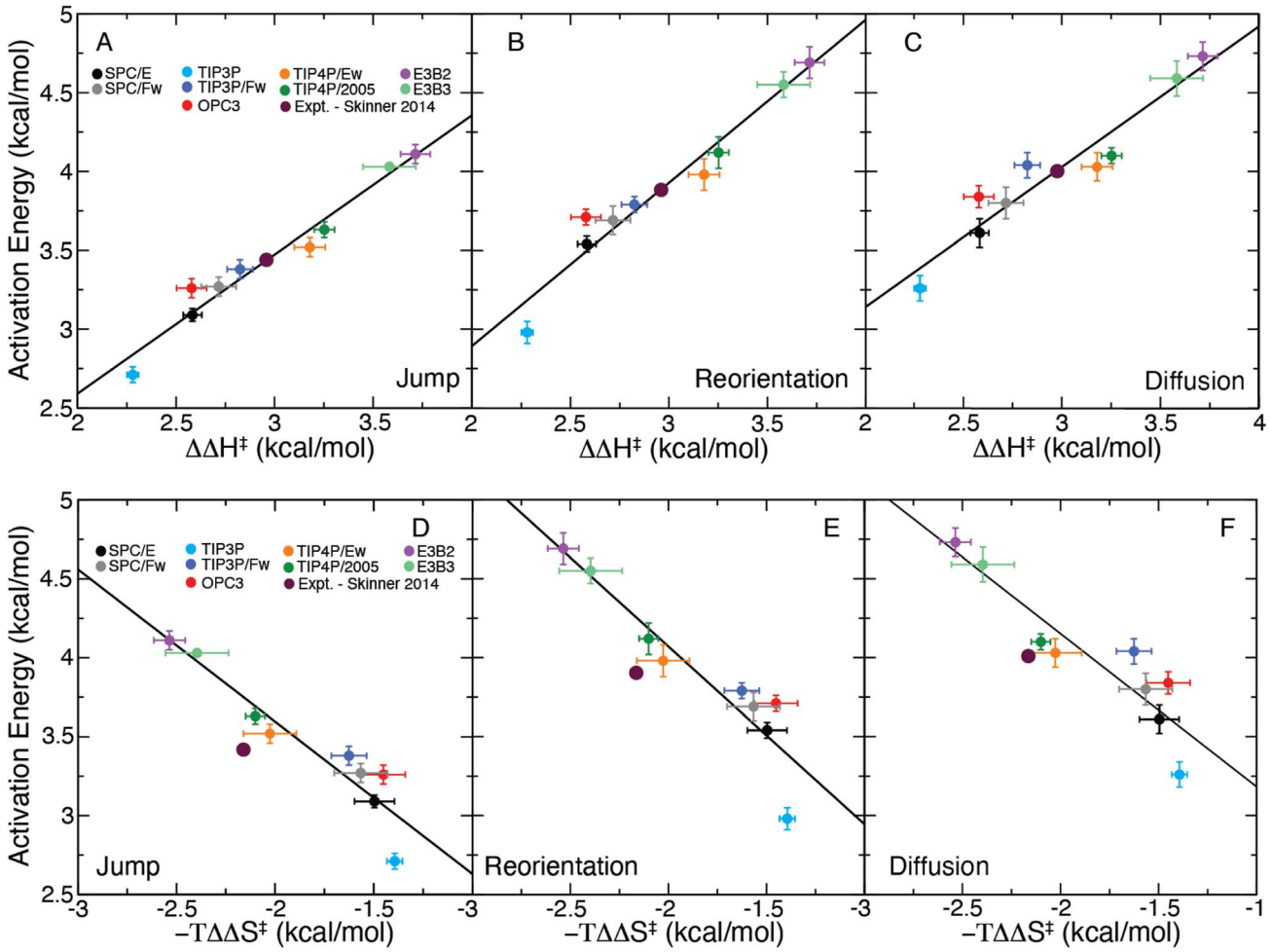

Fig. 4 Plot of the (A) jump, (B) reorientation, and (C) diffusion activation energies plotted for each water model as a function of $\Delta\Delta H^{\ddagger}$ and the same for $-T\Delta\Delta S^{\ddagger}$ (D–F). Linear fits are included for each panel as a solid black line. The predicted activation energies from the X-ray data of Skinner *et al.*,[43] generated using the correlations of $\Delta\Delta H^{\ddagger}$, are included on each plot.

energy is slightly different than one, which may be indicative of a temperature dependence of the H-bond jump transmission coefficient as well as the non-zero barrier in the jump angle. The same is true for the reorientation and diffusion activation energies, but this is expected because these processes involve contributions from "frame" motion between H-bond jumps as well as the magnitudes of the angular and translational motions with an H-bond exchange.[7,19,22,24] These factors also explain the slightly weaker correlations of $E_{a,2}$ and $E_{a,D}$ with $\Delta\Delta H^{\ddagger}$ compared to that for $E_{a,0}$. This strong structure–dynamics relationship will be used to determine $E_{a,0}$, which is not accessible experimentally, from $\Delta\Delta H^{\ddagger}$ determined from the temperature dependence of the measured RDF.

We have also calculated $-T\Delta\Delta S^{\ddagger}$, the entropic contribution to the free energy barrier corresponding to an H-bond exchange, which we have included in Table 1. With this a similar linear equation may be obtained as

$$E_{a,X} = m_{S,X}(-T\Delta\Delta S^{\ddagger}) + b_{S,X}, \quad (13)$$

where $m_{S,X}$ and $b_{S,X}$ are again the slope and intercept; their values are given in Table S2 in the ESI.†

We have plotted $E_{a,X}$ as a function of $-T\Delta\Delta S^{\ddagger}$ for each water model in Fig. 4D–F and fitted these data to eqn (13). While the observed correlations are strong (R^2 between 0.842 and 0.887), they are weaker than that found for the enthalpic correlations. (Full details of the fits are provided in Table S2.†) The strong linear correlations of the activation energies with $-T\Delta\Delta S^{\ddagger}$ is likely a direct result of enthalpy–entropy compensation in the water models.[62]

With these correlations in hand, we can use the experimental results of Skinner *et al.*,[43] which give $\Delta\Delta H^{\ddagger}_{expt} = 2.97$ kcal mol^{-1} and $-T\Delta\Delta S^{\ddagger}_{expt} = -2.16$ kcal mol^{-1}, to infer the activation energies. As the correlations with $\Delta\Delta H^{\ddagger}$ are stronger than with the entropy, we use $\Delta\Delta H^{\ddagger}_{expt}$ and our fitted parameters in Table S1† to estimate the activation energies from the experimental data. We first apply this approach to predict $E_{a,2}$ and $E_{a,D}$ as these have been previously determined experimentally. This provides a validation of the use of these structure–dynamics relationships to determine activation energies. We find an estimated value of $E_{a,2} = 3.89$ kcal mol^{-1}, which is in good

agreement with the values measured by Petersen *et al.*[28] (4.1 ± 0.5 kcal mol^{-1}) and Nicodemus *et al.*[29] (3.7 ± 0.5 kcal mol^{-1}). We also obtain an estimate of $E_{a,D} = 4.00$ kcal mol^{-1}, which is close to the range of 4.2–4.6 kcal mol^{-1} found in direct experimental measurements.[10,11,63,64] (The entropic correlations using $-T\Delta\Delta S^{\ddagger}_{expt}$ predict values of $E_{a,2} = 4.26$ kcal mol^{-1} and $E_{a,D} = 4.30$ kcal mol^{-1}; these values are also reasonable, but the stronger correlations with $\Delta\Delta H^{\ddagger}$ indicate those likely provide the better estimates.)

The fact that these estimates of $E_{a,2}$ and $E_{a,D}$ are in accord with direct measurements supports using the structure–dynamics relationship to determine the H-bond jump activation energy. This yields $E_{a,0} = 3.43$ kcal mol^{-1},[65] which to the best of our knowledge is the first estimate of this value based on experimental data. If we instead utilize the entropic correlations, we find that the jump activation energy is 3.76 kcal mol^{-1}, which is within uncertainty of the enthalpy-derived value.

6 Conclusions

In summary, we have used molecular dynamics simulations of nine commonly used water models to evaluate the connection between liquid structure and dynamics. We have calculated the RDF and the Gibbs free energy along with the enthalpic and entropic contributions to the free energy along the OO coordinate in water using fluctuation theory for each of the water models. We then demonstrate, using these data, that a strong linear dependence exists between the activation energies of three dynamical timescales (hydrogen-bond exchanges, OH reorientation, and water self-diffusion) and the enthalpic barriers involved in a hydrogen-bond exchange. Finally, we have used this structure–dynamics relationship to obtain the first experimentally-derived value of the H-bond jump activation energy from the measured T-dependent RDFs of Skinner and coworkers.[43] These results should motivate further temperature-dependent measurements of the water structure to better determine the H-bond jump activation energy by way of the thermodynamics of the water structure.

Data availability

The RDFs and RDF derivatives calculated for different water models have been deposited at Zenodo (**https://doi.org/10.5281/zenodo.10463858**).

Author contributions

The study was designed by all the authors. Simulations and data analysis were performed by Z. A. P. All of the authors wrote the paper.

Conflicts of interest

There are no conflicts to declare.

Acknowledgements

The authors would like to thank Prof. Brian B. Laird and Dr Steven Strong for many useful discussions. This work was supported by the National Science Foundation under Grant No. CHE-1800559 and CHE-2102656. This material is based on the work supported by the National Science Foundation Graduate Research Fellowship under Grant No. 1540502 and 1451148 as well as the National Science Graduate Research Opportunities Worldwide Program. The calculations were performed at the University of Kansas Center for Research Computing (CRC).

References

1 R. Rey, K. B. Møller and J. T. Hynes, *J. Phys. Chem. A*, 2002, **106**, 11993–11996.
2 K. B. Møller, R. Rey and J. T. Hynes, *J. Phys. Chem. A*, 2004, **108**, 1275–1289.
3 C. Fecko, J. Eaves, J. Loparo, A. Tokmakoff and P. Geissler, *Science*, 2003, **301**, 1698–1702.
4 D. E. Moilanen, E. E. Fenn, Y.-S. Lin, J. L. Skinner, B. Bagchi and M. D. Fayer, *Proc. Natl. Acad. Sci. U. S. A.*, 2008, **105**, 5295–5300.
5 E. Brini, C. J. Fennell, M. Fernandez-Serra, B. Hribar-Lee, M. Lukšič and K. A. Dill, *Chem. Rev.*, 2017, **117**, 12385–12414.
6 H. J. Bakker, Y. L. A. Rezus and R. L. A. Timmer, *J. Phys. Chem. A*, 2008, **112**, 11523–11534.
7 D. Laage and J. T. Hynes, *J. Phys. Chem. B*, 2008, **112**, 14230–14242.
8 C. H. Cho, J. Urquidi, S. Singh and G. W. Robinson, *J. Phys. Chem. B*, 1999, **103**, 1991–1994.
9 L. D. Eicher and B. J. Zwolinski, *J. Phys. Chem.*, 1971, **75**, 2016–2024.
10 L. A. Woolf, *J. Chem. Soc., Faraday Trans. 1*, 1975, **71**, 784–796.
11 K. Krynicki, C. D. Green and D. W. Sawyer, *Faraday Discuss. Chem. Soc.*, 1978, **66**, 199–208.
12 C. Rønne, L. Thrane, P. O. Åstrand, A. Wallqvist, K. V. Mikkelsen and S. R. Keiding, *J. Chem. Phys.*, 1997, **107**, 5319–5331.
13 J. Ortiz De Urbina and G. Sesé, *Phys. Rev. E*, 2016, **94**, 1–7.
14 J. Teixeira, M.-C. Bellissent-Funel, S. H. Chen and A. J. Dianoux, *Phys. Rev. A*, 1985, **31**, 1913–1917.
15 J. Qvist, H. Schober and B. Halle, *J. Chem. Phys.*, 2011, **134**, 144508.
16 B. J. Gertner, R. M. Whitnell, K. R. Wilson and J. T. Hynes, *J. Am. Chem. Soc.*, 1991, **113**, 74–87.
17 K. Ando and J. T. Hynes, *J. Mol. Liq.*, 1995, **64**, 25–37.
18 K. Ando and J. T. Hynes, *J. Phys. Chem. B*, 1997, **101**, 10464–10478.
19 D. Laage and J. T. Hynes, *Science*, 2006, **311**, 832–835.
20 Y. S. Lin, P. A. Pieniazek, M. Yang and J. L. Skinner, *J. Chem. Phys.*, 2010, **132**, 174505.
21 E. N. Ivanov, *J. Exp. Theor. Phys.*, 1964, **18**, 1247–1250.
22 A. Gomez, Z. A. Piskulich, W. H. Thompson and D. Laage, *J. Phys. Chem. Lett.*, 2022, **13**, 4660–4666.

23 Z. A. Piskulich, D. Laage and W. H. Thompson, *J. Phys. Chem. A*, 2021, **125**, 9941–9952.
24 Z. A. Piskulich, D. Laage and W. H. Thompson, *J. Chem. Phys.*, 2020, **153**, 074110.
25 D. E. Moilanen, D. Wong, D. E. Rosenfeld, E. E. Fenn and M. D. Fayer, *Proc. Natl. Acad. Sci. U. S. A.*, 2009, **106**, 375–380.
26 M. Ji, M. Odelius and K. J. Gaffney, *Science*, 2010, **328**, 1003–1005.
27 Z. A. Piskulich, D. Laage and W. H. Thompson, *J. Chem. Phys.*, 2021, **154**, 064501.
28 C. Petersen, K. J. Tielrooij and H. J. Bakker, *J. Chem. Phys.*, 2009, **130**, 214511.
29 R. A. Nicodemus, S. A. Corcelli, J. L. Skinner and A. Tokmakoff, *J. Phys. Chem. B*, 2011, **115**, 5604–5616.
30 H. Weingartner, *Z. Phys. Chem.*, 1982, **132**, 129–149.
31 S. H. Northrup and J. T. Hynes, *J. Chem. Phys.*, 1980, **73**, 2700–2714.
32 Z. A. Piskulich, O. O. Mesele and W. H. Thompson, *J. Chem. Phys.*, 2017, **147**, 134103.
33 Z. A. Piskulich, O. O. Mesele and W. H. Thompson, *J. Phys. Chem. A*, 2019, **123**, 7185–7194.
34 Z. A. Piskulich and W. H. Thompson, *J. Chem. Theory Comput.*, 2021, **17**, 2659–2671.
35 Z. A. Piskulich and W. H. Thompson, *J. Chem. Phys.*, 2020, **152**, 011102.
36 N. A. Mahynski, S. Jiao, H. W. Hatch, M. A. Blanco and V. K. Shen, *J. Chem. Phys.*, 2018, **148**, 194105.
37 J. I. Monroe, H. W. Hatch, N. A. Mahynski, M. S. Shell, V. K. Shen and N. A. Mahynski, *J. Chem. Phys.*, 2020, **153**, 144101.
38 M. P. Allen and D. J. Tildesley, *Computer Simulation of Liquids*, Oxford, New York, 2017.
39 A. H. Narten, W. E. Thiessen and L. Blum, *Science*, 1982, **217**, 1033–1034.
40 A. Soper, *Chem. Phys.*, 2000, **258**, 121–137.
41 T. Head-Gordon and G. Hura, *Chem. Rev.*, 2002, **102**, 2651–2670.
42 A. H. Narten and H. A. Levy, *J. Chem. Phys.*, 1971, **55**, 2263–2269.
43 L. B. Skinner, C. J. Benmore, J. C. Neuefeind and J. B. Parise, *J. Chem. Phys.*, 2014, **141**, 214507.
44 L. Martinez, R. Andrade, E. Birgin and J. Martinez, *J. Comput. Chem.*, 2009, **30**, 2157–2164.
45 S. Plimpton, *J. Comput. Phys.*, 1995, **117**, 1–19.
46 S. Nosé, *J. Chem. Phys.*, 1984, **81**, 511–519.
47 W. G. Hoover, *Phys. Rev. A*, 1985, **31**, 1695–1697.
48 T. Darden, D. York and L. Pedersen, *J. Chem. Phys.*, 1993, **98**, 10089–10092.
49 E. L. Pollock and J. Glosli, *Comput. Phys. Commun.*, 1995, **95**, 93–110.
50 J. P. Ryckaert, G. Ciccotti and H. J. Berendsen, *J. Comput. Phys.*, 1977, **23**, 327–341.
51 D. P. Shoemaker, C. W. Garland and J. W. Nibler, *Experiments in physical chemistry*, McGraw-Hill, New York, 1989.
52 H. J. Berendsen, J. R. Grigera and T. P. Straatsma, *J. Phys. Chem.*, 1987, **91**, 6269–6271.
53 Y. Wu, H. L. Tepper and G. A. Voth, *J. Chem. Phys.*, 2006, **124**, 024503.
54 W. L. Jorgensen, J. Chandrasekhar, J. D. Madura, R. W. Impey and M. L. Klein, *J. Chem. Phys.*, 1983, **79**, 926–935.
55 D. J. Price and C. L. Brooks, *J. Chem. Phys.*, 2004, **121**, 10096–10103.
56 S. Izadi and A. V. Onufriev, *J. Chem. Phys.*, 2016, **145**, 074501.
57 C. J. Tainter, P. A. Pieniazek, Y. S. Lin and J. L. Skinner, *J. Chem. Phys.*, 2011, **134**, 184501.
58 C. J. Tainter, L. Shi and J. L. Skinner, *J. Chem. Theory Comput.*, 2015, **11**, 2268–2277.
59 J. L. Abascal and C. Vega, *J. Chem. Phys.*, 2005, **123**, 234505.
60 H. W. Horn, W. C. Swope, J. W. Pitera, J. D. Madura, T. J. Dick, G. L. Hura and T. Head-Gordon, *J. Chem. Phys.*, 2004, **120**, 9665–9678.
61 D. M. Wilkins, D. E. Manolopoulos, S. Pipolo, D. Laage and J. T. Hynes, *J. Phys. Chem. Lett.*, 2017, **8**, 2602–2607.
62 S. W. Rick and W. H. Thompson, *J. Chem. Phys.*, 2023, **158**, 194504.
63 R. Mills, *J. Phys. Chem.*, 1973, **77**, 685–688.
64 K. T. Gillen, D. C. Douglass and M. J. Hoch, *J. Chem. Phys.*, 1972, **57**, 5117–5119.
65 Due to the different factors involved in this estimate it is difficult to directly calculate the uncertainty in this value, but we expect it is $\sim$0.60 kcal mol^{-1} based on approximate propagation of errors.